5-2014

ADAPTATION OF GAMMA CAMERA SYSTEM FOR SMALL FIELD-OF-VIEW APPLICATIONS

Melanie Carroll

Adaptation of Gamma Camera System for Small Field-of-View Applications

by

Melanie Carroll

Undergraduate Honors Thesis under the direction of

Dr. Kenneth Matthews

Department of Physics and Astronomy

Submitted to the LSU Honors College in partial fulfillment of the Upper Division Honors Program

May 2014

Louisiana State University
& Agricultural And Mechanical College
Baton Rouge, Louisiana

Table of Contents

Acknowledgments

I first thank Dr. Kip Matthews for working with me for four years. Your patience and persistence kept me going when the project was stalled or nothing was working. I truly appreciate your willingness and efforts to direct this work.

I also thank my committee members: Dr. Mette Gaarde and Dr. Kyle Harms. Your feedback and advice on this thesis was truly invaluable. Brad Ellison, the Physics Electronics Shop, and the Machine Shop were extremely helpful in manufacturing, modifying, and debugging components. I am grateful for the advisors in the Honors College, particularly Dr. Granger Babcock and Marybeth Smith, as well as in the College of Science.

To my family and friends, this work would not have been completed without your continued support. I especially thank my parents, John and Mary Carroll, for raising me to be an overachiever.

List of Figures

Abstract

Small field-of-view gamma ray imaging systems have a variety of applications in medicine, including intraoperative imaging. A key requirement is to decrease the bulk and weight of the detector system to facilitate ease of portable operation. Semiconductor detectors like cadmium zinc telluride (CZT) are preferred because of their compact size and energy resolution. An early prototype portable CZT imaging system has been modified by designing a new detector head to further decrease its size and improve its utility for portable and intraoperative operation. The detector front-end consists of four CZT detector modules with signal amplifying electronics inside a tungsten case; the detector head interfaces with additional signal processing and computer interface electronics. Amplifiers prevent signal loss from occurring in the long cable connecting the detector to the external electronics. New components that have been developed for this detector include a detector carrier board and a signal routing board. The detector carrier board holds the sockets into which the CZT modules connect. This board interfaces to the signal routing board, which amplifies the signal for transmission to the external electronics. Other new components include a frame to hold the circuit boards, heat sinks, and a high voltage source inside the case. Future work for the small field-of-view detector system will be assessing its performance and using the system in a clinical research project.

1. Introduction

Medical imaging in the 20th century has benefitted from many technological advances and increasingly specialized applications. Imaging modalities such as computed tomography (CT) and magnetic resonance imaging (MRI) are perhaps the most well known and widely used, but these images primarily display anatomic information and lack physiological information. Nuclear imaging, on the other hand, fundamentally differs from other modalities because of its dependence on the body to interact with radiopharmaceuticals. The introduction of positron emission tomography (PET) and single-photon emission computed tomography (SPECT) allowed physicians to visualize physiological processes, such as identifying tumors based on their metabolism.

Nuclear imaging depends on a pharmaceutical attached to a radioisotope that is injected into the body where it localizes in a tumor or other specific site. The radiation emitted by the radioisotope is detected by a gamma camera; the location of the radiopharmaceutical is shown as an image based on many detected gamma rays. Commercial gamma cameras are available in a variety of sizes, the most common being full-body scanners (Figure 1). Small field-of-view devices can be more patient-friendly and mobile, allowing physicians to reduce the distance between the detector and the patient which gives higher quality images. Additionally, probe-sized detectors are more practical for some applications in medical diagnosis and treatment, such as localizing cancers in the prostate and radioguided surgery[1,2,3]. Radiation imaging systems also have applications outside of medical imaging, such as in astrophysics and homeland security[4, 5].

Figure 1. Commercial gamma camera. The two detector heads (above and below) produce a full-body scan with "hot" spots indicating where a radiopharmaceutical has accumulated.

1.1 Scintillation and semiconductor cameras

Gamma cameras are commonly constructed from sodium iodide (NaI) crystals which scintillate after absorbing a gamma ray, hence the alternate name of scintillation camera. Photomultiplier tubes (PMTs) convert the scintillation light into charge-based signals. NaI and PMTs result in a bulky and heavy detector due to the large volume that must be shielded and the weight of the shielding and collimator (Figure 2). Thick crystals are desirable for good detection efficiency, but increasing the crystal thickness worsens intrinsic spatial resolution. While the energy resolution of NaI detectors is adequate for gamma ray imaging of many radiopharmaceuticals, improved energy resolution leads to better image quality because of improved identification and rejection of gamma rays that have Compton scattered in the object. The widely used Tc-99m radioisotope has an energy peak at 140 keV; Co-57 is often used for detector testing because of its similar energy peaks (122 keV and 136 keV)[6]. The $\Delta E/E$ energy

resolution of 10% for NaI detectors that is typical in this energy range means the two Co-57 peaks can't be distinguished separately.

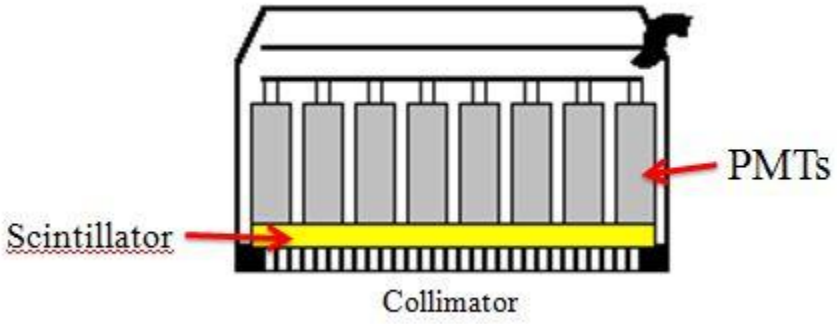

Figure 2. Illustration of a gamma camera based on a NaI scintillation detector. Gamma rays are converted in a two-step process: first to light by the scintillator, then to an electrical signal by the PMTs. Note that most of the volume of this detector is due to the PMTs.

Alternative radiation detectors were sought to reduce the bulkiness of scintillation cameras. Thus attention was turned to semiconductor radiation detectors. Semiconductors are typically dense and have a high effective atomic number, both of which improve gamma ray absorption efficiency. Another important parameter is the Fano factor, an intrinsic characteristic related to noise that influences energy resolution. These properties vary among semiconductors which affect their performance as radiation detectors. A drawback to semiconductors is that they are substantially more expensive to manufacture in terms of cost per unit area.

Absorption of ionizing radiation within a semiconductor material produces electron-hole pairs; the number of charge carriers created depends on absorbed energy (Figure 3). Using a strong electric field, transport of electron-hole pairs induces a pulse of charge. Semiconductors thus directly convert gamma rays into charge-based signals, a single-step process as compared to

the two-step process in scintillation detectors. Because semiconductors do not require PMTs, overall detector size is reduced and less radiation shielding is required.

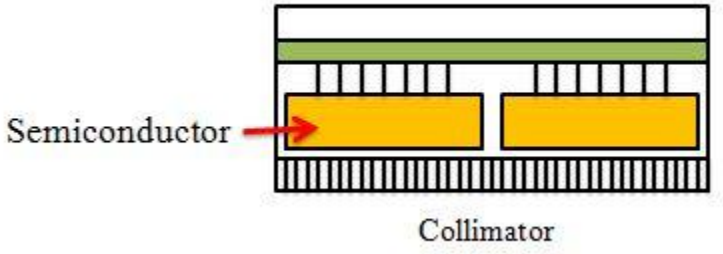

Figure 3. Illustration of a semiconductor detector system. The gamma ray is converted to an electrical signal in a single step process.

Semiconductors typically have better energy resolution than scintillation detectors because of the direct conversion and a small Fano factor. Typical energy resolution for gamma cameras is 9-10%, although CZT detectors have achieved 6.5% resolution at 122 keV[7]. These detectors will be able to differentiate the 122 keV and 136 keV gamma rays from Co-57. This means that semiconductors are better able to separate primary (uninteracted) gamma rays from Compton scattered photons; as mentioned, improved scatter rejection will improve image quality.

1.2 Recent progress in CZT imaging systems

Cadmium zinc telluride (CZT) is a promising material for a semiconductor radiation detector. The addition of zinc to cadmium telluride (CdTe) compounds raises the band gap and resistivity of the material but lowers the density. Extensive research has been conducted on the properties of CZT crystals and how those properties affect the performance as gamma ray detectors. Crystals can be grown using several methods, the most common being the vertical Bridgman and traveling heater methods[8]. These crystals can be characterized using a synchrotron

X-ray beam through micro-scale detector mapping, diffraction topography, and etch-pit density analysis[9]. These methods reveal structural defects at the microscopic level that affect imaging performance. Tellurium inclusions must have a small size and low concentration or else the energy resolution of the detector suffers[5].

CZT detectors are valued for their ability to operate at room temperature with high energy resolution, high spatial resolution, and low leakage currents[4]. The relatively high atomic numbers of cadmium and tellurium (48 and 52, respectively) make CZT more efficient at absorbing gamma rays than other common semiconductor detectors, such as silicon and germanium[8]. Additionally, silicon and germanium detectors require cooling by liquid nitrogen and cannot be operated at room temperature, which is impractical for clinical use[4]. Higher efficiency leads to lower doses and shorter acquisition times for patients, which is both prudent and convenient[10]. Due to its higher density and effective atomic number, a thinner amount of CZT results in an equivalent detection efficiency as a thicker piece of NaI.

Recent work on CZT gamma cameras includes a wide range of medical and non-medical applications. CZT detectors with three-dimensional detection were reported for the location of landmines[11]. Small CZT detectors have been investigated for cardiac and breast imaging, with at least one commercial CZT imaging system now available for breast imaging (GE, Discovery NM750b)[3, 12]. Current practice in radioguided surgery uses non-imaging gamma probes to locate malignant tissue or sentinel lymph nodes for excision. These probes use variable pitch audio output to alert the user. CZT detectors provide an option for intra-operative imaging; devices in testing can produce images that may be useful in lymph node biopsy[3]. Similarly, a transrectal detector has been used to identify cancerous regions of the prostate in a procedure that was well-

tolerated by patients[1]. These examples show the diverse applications available for small field-of-view detectors.

1.3 Motivation and goals

The motivation for this work was to construct a small field-of-view CZT gamma camera that can be used for intraoperative imaging, small animal imaging, or other applications appropriate for a compact gamma-ray imaging system. A long-range goal for this detector is its use for pediatric pancreatic imaging with colleagues at the LSU Health Science Center – Shreveport. This detector could also be useful for imaging mice and rats with colleagues in the LSU School of Veterinary Medicine.

The focus of this project was the development of the detector head itself. To facilitate development, some electronics, other hardware, and software from existing CZT and scintillation gamma camera prototypes were utilized. The detector head comprised a carrier board for the CZT modules, a signal routing board for immediate processing of some signals generated by the modules, a high-voltage source, passive detector cooling, a collimator, and tungsten shielding. The carrier board, signal routing board, and cooling assembly were developed specifically for this project, along with modifications to the reused portions of the two previous systems. A list of components and their related tasks is enumerated below.

- Detector Carrier Board
    - Board layout
    - Fabrication
    - Population
    - Testing
- Signal Routing Board
    - Board layout
    - Fabrication
    - Population
    - Testing

- Canister
    - High voltage plane
    - Heat sinks
    - Frame
    - Back cover
- DAB modification
    - Removal of components
    - Testing
- Software modification
    - Global module number
    - Initialization file

Chapter 2 describes the relevant aspects of the existing detector systems; Chapter 3 describes the development work specific to this project. Chapter 4 will discuss problems that have been overcome and the current status of the detector system.

2. LabRAT CZT Gamma-ray Imaging System

The Laboratory Radioactive Assay Tracer (LabRAT) was a bench top CZT gamma-ray imaging system (Mosaic Imaging Technology, Inc.). Two versions of the device existed and this project used portions of the updated Version 1 (Figure 4). The system consisted of two aluminum boxes, approximately 31 cm x 31 cm x 27 cm, connected by a ribbon cable and power socket. The bottom unit contained power supplies and processing electronics, while the top unit contained the detector modules mounted in an aluminum framework and a high voltage supply. LabRAT utilized CZT modules (Imarad LTD) that each contained a monolithic crystal, two application-specific integrated circuits (ASICs), and a circuit board to route data signals and power. Each module contained an array of 16 x 16 pixels of size 2.4 mm x 2.4 mm x 5 mm. LabRAT held up to twenty-five modules in a 5 x 5 array. The head unit also contained a large square copper foil for high voltage distribution across the face of the CZT modules.

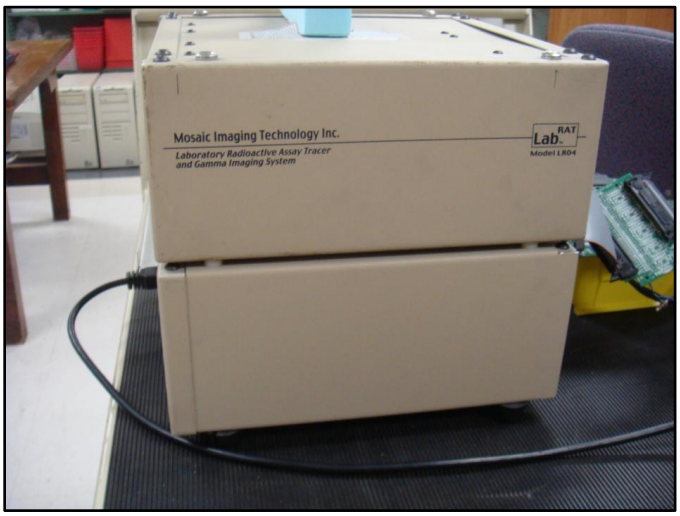

Figure 4. LabRAT detector DFE (top) and base unit (bottom).

LabRAT was used as the basis for this project because its accompanying software and performance had been previously investigated and optimized. This system also presented a logical approach to being adapted for a small field-of-view application, namely, replacing the

detector head with a portable version that can interact with the base in the same fashion as the original. LabRAT is described in the following sections, to identify those signals and components that were replicated or modified for the new system.

2.1 Detector Base Unit

The bulk of the volume of the base of LabRAT was taken up by power supplies: +24 V for the high voltage supply, ±5 V (digital) and ±5 V for signal processing electronics, and ±2 V for the CZT modules. All three sources had their grounds connected at key locations to prevent uneven or floating grounds. Power for the high voltage and CZT modules was supplied to the head unit through a fifteen pin socket that directly connected the two units together.

The other components housed within the base unit were the Detector Acquisition Board (DAB) and Detector Link Board (DLB) (Imarad LTD), shown in Figure 5. The former converted detector outputs to voltages, sampled the signals, and stored them in digital memory. The latter fetched digitally stored data from the DAB and then converted and transmitted it to the host computer. These circuit boards were connected by two sockets so that the DLB sat atop the larger DAB. The DAB connected to the Detector Front End (DFE), which held the CZT modules in the detector's head unit, by a 40-pin ribbon cable.

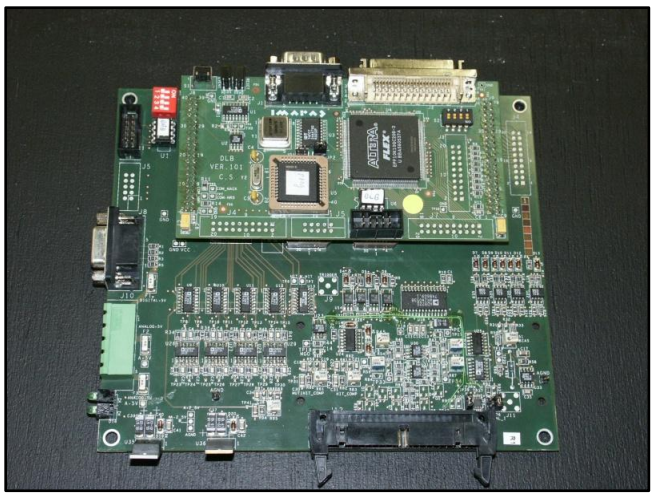

Figure 5. Photograph of the DAB and DLB. The pale green socket on the left side is the power connector and the ribbon cable connector at the bottom sends and receives signals from the detector head unit (DFE).

Because the DAB receives outputs from the detector modules, its components were most important for this project. In particular, three types of signals were identified that would have to be handled appropriately when building a new detector head unit: the trigger signal, the event signals, and the address signals; other command and control signals could be used without modification. These signal types were each current signals which are degraded over any appreciable cable lengths between the base and head units; current-based signals must be converted to voltage-based signals for transmission as well as for subsequent signal processing. The DAB and DFE were originally designed to be located in close proximity, connected by a short length of cable, so all signal processing electronics had been placed on the DAB itself (Figure 6). However, for compactness it was desirable for the DAB and the detector head to be separated from each other, connected by a long length of cable. Thus, a portion of the DAB's electronics had to be moved into the new detector head unit.

The trigger notified the computer when an event had occurred and was used to establish when more than one event occurred simultaneously. The CZT modules were designed to output a

trigger signal labeled “MGO” with an amplitude of 60 microamps or a multiple thereof. After processing by comparators on the DAB, this signal produced two outputs called “Trigger” and “Multihit”. The former signified that an event had occurred while the latter established that two events occurred within a predetermined time (“pileup”). Both signals were connected to orange LEDs on the DAB so that visible confirmation of an event was possible. The multihit signal was necessary because when two gamma rays interact with the module nearly simultaneously, the device recorded the sum of the energies, misinterpreting two events as one event with a much larger energy without the multihit signal.

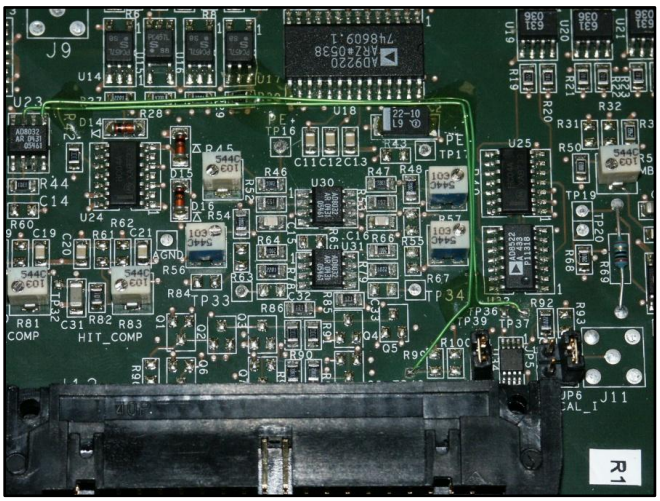

Figure 6. Close-up photograph of the energy signal circuits, center. The lower op-amp (U31) was the current-to-voltage converter and the op-amp immediately above it (U30) provided the necessary offset for each. The trigger op-amp is also visible at the top far left (U23).

The amount of energy deposited in the detector by a gamma ray generated two signals that were identical except for polarity, one as a positive polarity and the other as a negative polarity. The energy signals from the detector module ranged from zero to ±200 μA. The DAB electronics converted these energy signals into differential signals, which increased the accuracy and maximum range of the energy measurement. Amplifiers on the DAB (Figure 6) converted

the current signals from the detector module to voltage signals and then offset the signals so that their baseline voltages were complementary while their peak voltages were inverses of each other, as shown in Figure 7 (yellow and blue signals). The positive energy signal had a base voltage at ground and a maximum voltage of approximately 500 mV. The negative energy signal had a base voltage of 500 mV and a maximum voltage at ground. The task of offsetting these signals was accomplished by another op-amp. Only the part of these circuits for current-to-voltage conversion needed to be moved to the new detector head.

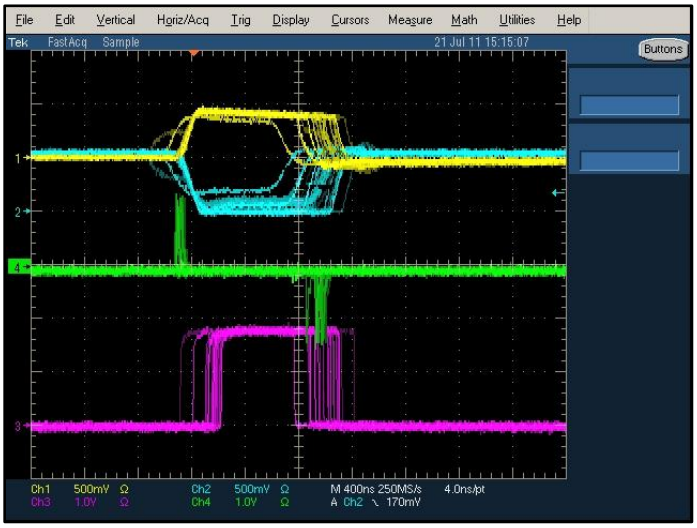

Figure 7. Image captured from Tektronix TDS 5054 Digital Phosphor Oscilloscope showing signals of interest for this project. While this image was captured with LabRAT, the signals from the new detector must be identical. Blue: Negative energy. Yellow: Positive energy. Green: Address. Purple: Trigger.

The address signals recorded a unique identification number for each pixel, allowing the formation of a map showing how many events were counted in each pixel. Sixteen address signals were allocated to form a 16-bit address; 7 bits identified each pixel on an ASIC, 1 bit was used to identify which of the two ASICs on a CZT module, and the remaining 8 bits allowed for identification of individual modules (theoretically for a detector with up to 256 modules although LabRAT had 25 modules maximum and the new detector head had 4 modules). The current

signal from the module for each address line ranged from zero to 100 μA. To convert these current signals to voltage signals, four amplifiers with four channels each on the DAB (Figure 8) were utilized in a fashion similar to both the trigger and energy signal processing. Again, these current-to-voltage conversion amplifiers needed to be moved to the new detector head. While the energy and address signals had roughly the same gain from amplification, the trigger signal had less gain than either. After conversion, the address signals went to comparators to identify each address line as "on" (1) or "off" (0) to specify the pixel address.

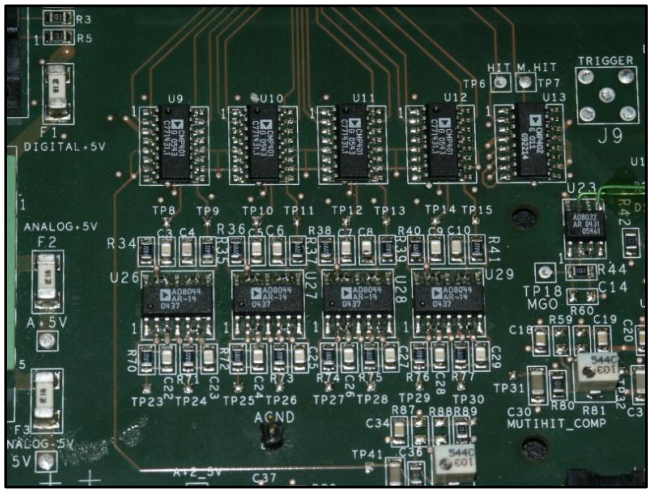

Figure 8. Close-up photograph of address signal circuitry on the DAB. Four lower amplifiers (U26 – U29) converted the signals from currents to voltages using a negative feedback loop. The signals then proceeded to comparators (U9 – U12) which are visible above the amplifiers.

These three signals – trigger, event, and address – were crucial for communication between the CZT modules and DAB. While the new detector head was designed to be compatible with LabRAT's existing DAB, some modifications were necessary to allow the new detector to be functional. The new detector head would duplicate the charge-to-voltage circuits already located on the DAB so those circuits were removed from the DAB and jumper wires were installed. For the address and trigger signals, the jumper wires led directly to comparators. For the two energy signals, the jumper wires led to the operational amplifier that offsets the base

voltage for each. All of these modifications were made to a spare DAB from a previous project. LabRAT's own DAB was not modified in any way and acted as a reference for this project.

2.2 Detector Front End

The DFE of LabRAThoused the Detector Carrier Board (DCB), which held an array of up to twenty-five CZT modules as shown in Figure 9, and a high voltage supply (Spellman). The voltage supply was adjustable between 0 and -1500 V from a +24 V input; the high voltage supply was set for -600 V. This voltage was applied to the face of the detectors via a cable connected to a large square of copper foil. Each module had a copper grid on its face and used the high voltage bias to generate a signal from each gamma-ray interaction. More explicitly, the applied voltage caused signal induction from transport of the electron-hole pairs through the semiconducting material.

4	5	14	15	24
3	6	13	16	23
2	7	12	17	22
1	8	11	18	21
0	9	10	19	20

Figure 9. Module numbering system for LabRAT. The bottom left corner corresponds to the corner closest to the signal cable connector on the physical board.

The CZT modules could populate the DCB in any desired configuration. The numbering of the modules within the array was important so that an image could be accurately recreated. Since each module contained two ASICs, the module number and ASIC number together corresponded to a specific position within the overall array. During initialization, the LabVIEW

software sequentially assigned the identification number to each ASIC. The numbers did not have to be consecutive; the LabVIEW code assumed the module numbering scheme in Figure 9 to facilitate building the image of detected gamma rays. For example, with the board populated with four detectors as shown in Figure 10, the modules are in positions 7, 8, 11, and 12. Thus, the corresponding ASIC values would be 14, 15, 16, 17, 22, 23, 24, and 25.

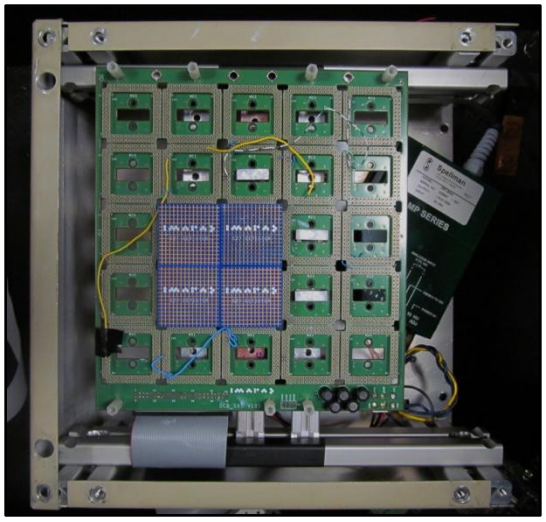

Figure 10. Inside view of LabRat's DFE. The DCB is populated with four Imarad CZT modules. On the right, the high voltage source is partially visible. The ribbon cable on the bottom left connects the DCB to the DAB. The yellow and blue wires bypass unused sockets.

If the array was not entirely filled with modules, wires were added to bypass unused sockets on the DCB. This was important because the initialization sequence loaded data serially into each ASIC; the daisy chains between the correct pins essentially skipped over sockets that were unoccupied. Another setting related to the number of modules was the DFE's main bias. The amplitude of the main bias was proportional to the number of modules in use. The main bias required 10 mV per detector, and was set over a 10 Ω resistor on the main bias amplifier on the DAB.

The DFE of LabRAT was designed to sit above the base unit so that the power socket between the two was connected and held in place by the weight of the head unit. Because the two units were identical in size, the DFE constituted half of the overall volume of the detector; much of the DFE's volume was wasted space. The new compact system replaced the LabRAT DFE but utilized the same base unit with a modified DAB.

2.3 LabView Interface

The DFE and base unit of LabRAT were controlled through LabView 8.0 (National Instruments). The software included programs to perform a variety of functions, including initializing the detector, setting parameters such as acquisition time or counts, and displaying the results. The software was developed in-house for a previous project with LabRAT[13]. Each program will not be discussed in detail, but those responsible for manipulation of key variables for standard operation will be described.

The front panel of LabView, shown in Figure 11, was the main point of contact between the user and LabRAT. The front panel was used to control initialization and communication parameters, to set acquisition limits and to manually start/stop the detector, to display measured count rates and energy spectra, and for debugging purposes. A supplemental window (not shown in Figure 11) was used to display images.

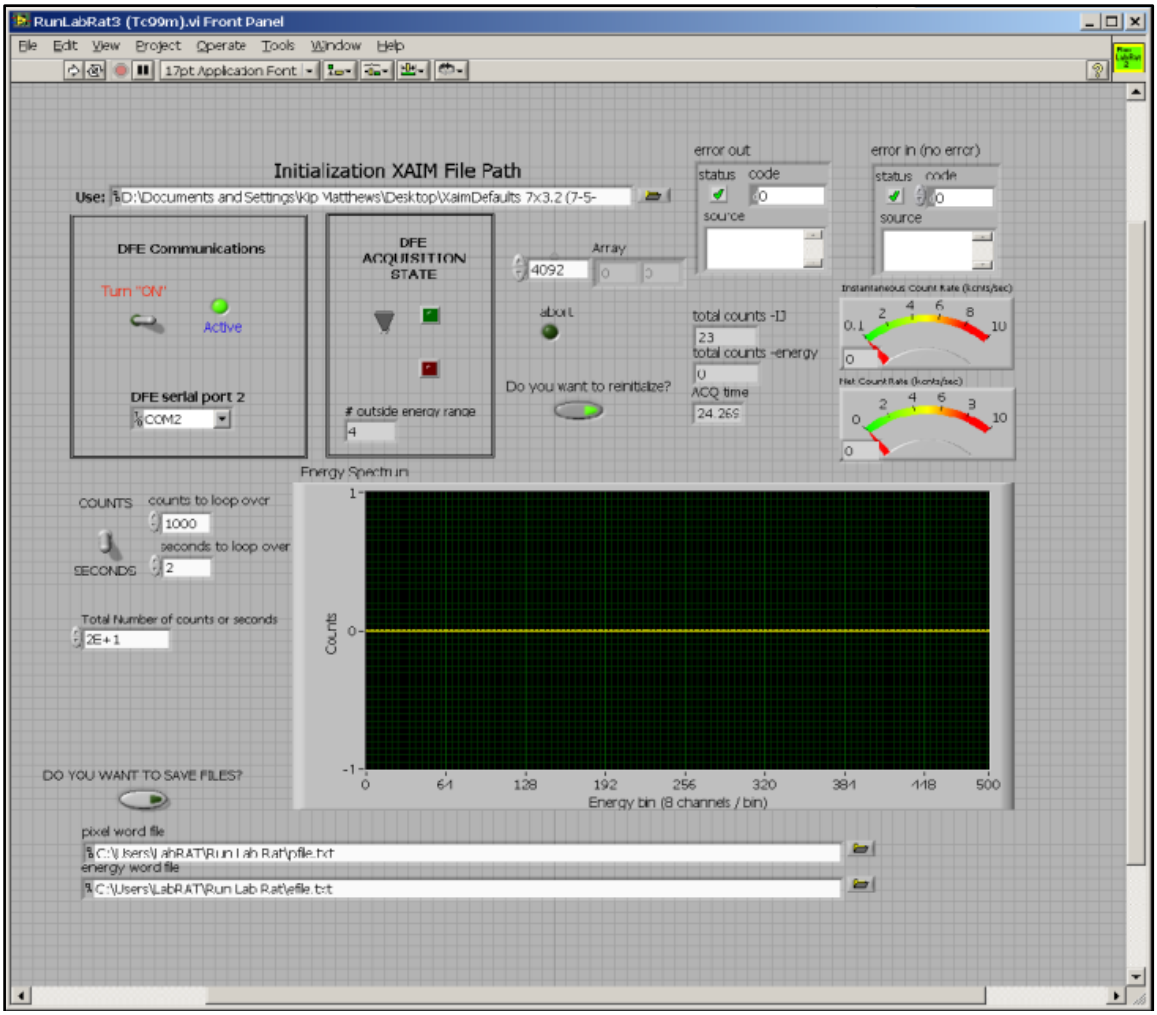

Figure 11. Front panel of the LabVIEW software for LabRAT.

The software provided a mechanism to initialize or to reinitialize the detector; LabView prompted the user for a predefined initialization file ("Initialization XAIM File Path"). If the user chose to do so, the initialization data could be updated through a pictorial representation of each ASIC. Scrolling through the various ASICs allowed the user to change any parameter within the initialization file without opening or saving the file itself. Ideally, the initialization file contained information for each ASIC present in LabRAT. If the initialization file contained information for too many or too few ASICS, the system would initialize but might not operate correctly or place

data in the correct image pixels. After saving any desired changes, the software implemented those changes to the detector.

Nuclear images are typically acquired for either a fixed duration or a specified total number of counts. At the middle left of the interface, a toggle switch and the text box below it allowed setting the stop condition to total counts or acquisition time. Two adjacent boxes controlled the number of counts or seconds between screen updates. At the bottom of the front panel, the user had the option to save the energy and address outputs in text files. These text files contained a value for each event, either the energy magnitude or the pixel address.

The plot in the center of the front panel displayed the energy spectrum of all events encountered, with the energy on the horizontal axis and the number of counts at that energy on the vertical axis. The plot is empty in Figure 11 because the screenshot was taken before LabRAT had acquired any data. A typical energy spectrum, shown in Figure 12, exhibits a characteristic tall peak for detected primary gamma rays and a low-energy tail representing the detection of gamma rays that scattered in the object or the detector. Running the device over a longer time or for more counts would result in a cleaner energy spectrum due to counting statistics.

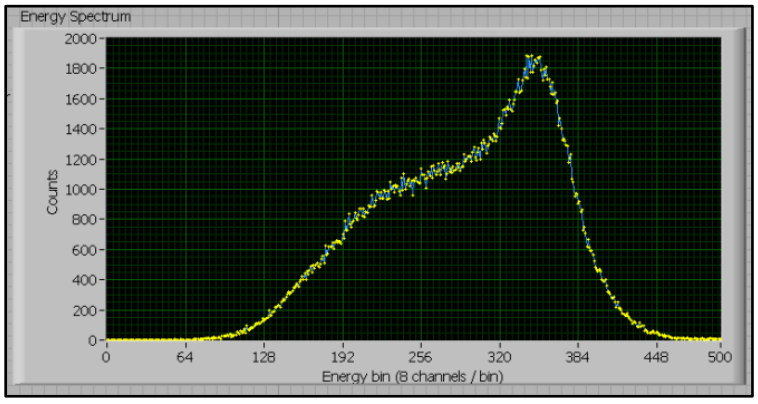

Figure 12. Energy spectrum display after running LabRAT.

The other output of the LabRAT software after running the detector was the image display. This display showed the number of counts for each picture on a color scale, with black being the least number of counts, white being the largest, and shades of blue being values in between. The location of each pixel was determined from the 16-bit address generated by the ASIC. This output is vital for most applications of the detector system, namely, visualizing the distribution of a gamma ray source within the body or other area of interest.

3. Compact CZT Gamma-ray Imaging System

The compact system was designed to replace the DFE of LabRAT but retain the same functionality (Figure 13). This included using the same CZT modules, part of the processing electronics, the power supplies, and the computer and software interface. New components dealt with support of the CZT modules and moving the rest of the processing electronics to the new detector head. Some key obstacles to address in developing the new system were manufacturing new boards to hold the detectors and electronics, deciding which electronics processing to include in the new head unit, and maintaining the ability to interface between the base unit and the new DFE.

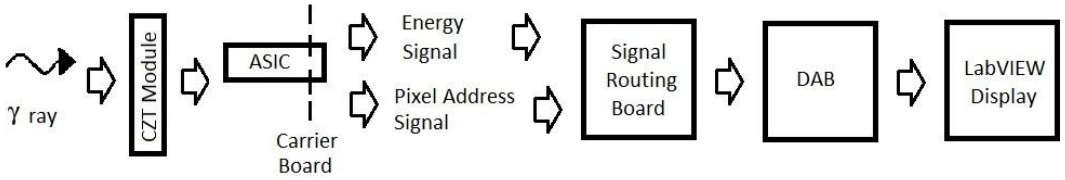

Figure 13. Flowchart of detector system components. This simplified diagram shows how the detector converts a gamma ray to an electrical signal and how that signal is processed and displayed.

The new detector head included two new circuit boards: a DCB to house the CZT modules and a signal processing board to provide preliminary processing for the three signals previously discussed. The two new boards sat piggy-backed in a tungsten canister, forming the DFE of the new detector system. Ancillary components in the new DFE included connectors for power and signals, a high voltage power supply for the detector modules, and an aluminum frame to form a heat sink system. Each of these components is discussed below.

3.1 Detector Carrier Board

The detector carrier board housed four CZT modules and measured 86 mm x 86 mm (Figure 14). The board's design was based directly on the board from LabRAT's DFE, merely on a smaller scale; the board layout was implemented by the Physics Electronics shop and fabricated by an outside vendor. The values for the discrete components were available from circuit schematics provided by the manufacturer. These components served a variety of functions, including protecting against power spikes and impedance matching. Four sockets were added to mount the detector modules. These sockets fit the pins from the ASICs, which were located on the boundary of each square module in two rows. Two single-row twenty-pin connectors were located on either side of the board to carry signals and ±2 V power to the modules. The screw holes in each corner connected this board to the signal routing board and ultimately to the rest of the frame.

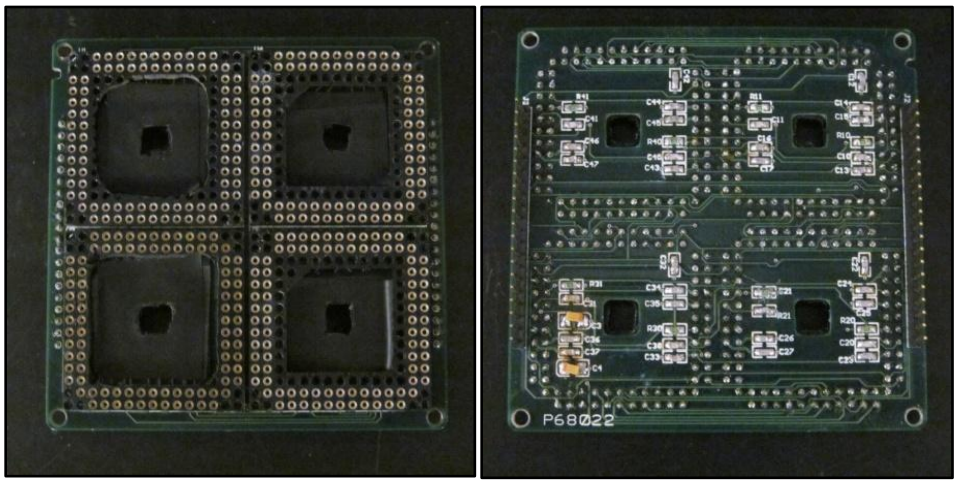

Figure 14. New compact detector carrier board. The front of the board (left) had sockets which held the CZT modules. The four holes in the center of each socket allowed for the heat sink to pass through. The back of the board (right) had electrical components and connectors which fit into sockets on the signal routing board.

Although signals were not processed on this board, each CZT module required complex connections to run properly. The connections for each pin were available on schematics from LabRAT. Like the original DCB in LabRAT, all signals were connected in parallel except for the serial initialization chain. Since each module contained two ASICs, each signal was connected in parallel to eight pins out of the four sockets. On each socket, as viewed in Figure 14(left), the top and right rows of pins were connected to one ASIC while the bottom and left rows of pins were connected to the other.

The order of the modules began with module 0 in the top left corner in Figure 14 and proceeded in a counter-clockwise direction. The four cutouts in the board allowed for heat sinks to pass through the board and come in contact with the back of the module. The heat sinks screwed into an aluminum frame, which allowed for adjustment to ensure that the heat sinks were in good contact with the modules. Electrical tape was added to provide some cushioning and prevent the heat sink from contacting the circuit board.

The detector carrier board replaced the equivalent board from the DFE of LabRAT, thereby fulfilling the same purpose. However, some differences between the two boards existed, the most obvious being the size. This size directly related to the field of view of the detector. Whereas LabRAT was intended for scintimammography with a potential maximum field of view of 19 cm x 19 cm, the new system was designed for intraoperative imaging with a maximum field of view of 76 mm x 76 mm. Thus, the field of view for the new detector was less than one quarter the area of LabRAT's field of view.

Another difference between the new detector carrier board and LabRAT's equivalent was the connectors utilized for signals and power. LabRAT used two separate connectors: a fifty-pin ribbon cable for signals and a separate socket for power for the modules (±2 V and ground). The

ribbon cable connected to another board located in the base unit which converted signals from the fifty-pin cable to a forty-pin cable that then carried signals to the DAB. For the new system, the simplest design would have been a forty-pin cable connecting the new detector carrier board and DAB directly. However, this cable would be fairly long (about six feet) to permit use of the system in its desired application. Current signals traversing a cable of this length would be irreversibly degraded and likely unusable upon their arrival at the DAB. Instead, the detector carrier board had two twenty-pin connectors which carried both signals and power for the modules. These connectors interfaced with a new signal routing board (see below).

While the differences between the detector carrier board and its predecessor shed light on important distinctions between the two systems, the similarities allowed the new system to function. The connections to each ASIC were matched exactly to allow the CZT modules to be used in either system. The layout of sockets and discrete components was also very similar between the two boards, simply because of the requirement of cutouts in the new DCB for heat sinks. In LabRAT, these holes were larger and rectangular whereas they were smaller and square for the new system due to the restricted size of the new DCB. The heat sinks are discussed in a later section.

3.2 Signal Routing Board

The signal routing board (Figure 15) provided preliminary processing for the three signals originating from the modules, as discussed in the previous chapter. This processing was crucial because the current signals from the CZT module would be degraded over any appreciable cable lengths. The preliminary processing used operational amplifiers (op-amps) to convert the current signals to voltage signals which are more stable over the same distance. In

total, six op-amps were used for this process: one for the trigger signal, one for the two energy signals, and four for the sixteen address signals.

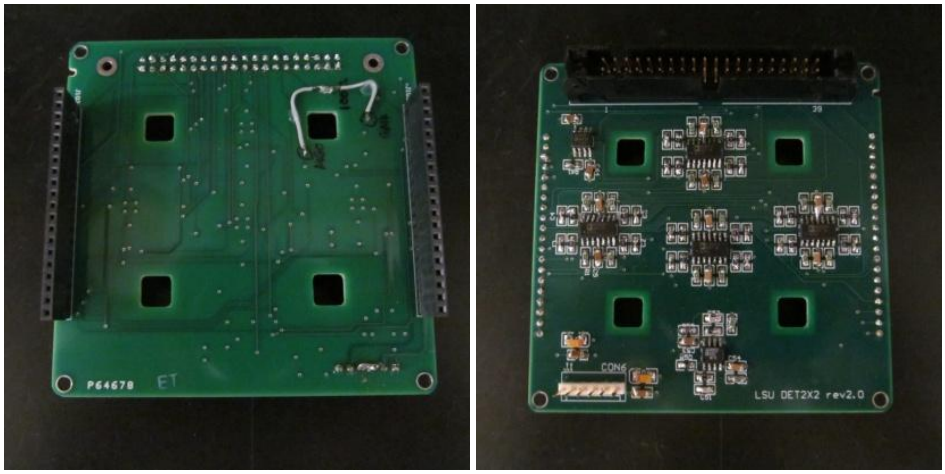

Figure 15. Signal routing board. The front (left) piggybacks to the back of the detector carrier board using the two sockets on either side. The back (right) holds the amplifiers, power connector, and signal cable connector. The four heat sink holes align with those on the detector carrier board.

The board had two twenty-pin connectors to mount to the detector carrier board, as well as a forty-pin signal connector and a six-pin power connector. The forty-pin connector transported signals via ribbon cable to the existing DAB from LabRAT. These signals included those from the output of the amplifiers on this board and the initialization data directly to each ASIC. To maintain interfacing ability, the signals at each pin corresponded to those from the original LabRAT schematic. The six-pin connector provided ±5 V to the amplifiers, ±2 V to the modules, and a common ground.

Two models of op-amps were used on the signal routing board: the two-channel AD8032 (Analog Devices) for the energy and trigger signals and the four-channel AD8044 (Analog Devices) for the address signals. Each op-amp used ±5 V for power. The op-amps used negative feedback to improve the characteristics of the incoming signal such as amplitude and noise. Two major principles are at work in op-amps: the voltage difference between the two inputs is zero

and the inputs draw no current[14]. These op-amps were operated as inverting charge-to-voltage convertors; with the input of a small current-based signal, the output had the opposite polarity and an amplified voltage magnitude proportional to the input current.

The basic processing for each signal was the same (Figure 16): the signal entered at the inverting input of the op-amp and a feedback loop connected the output to the signal input. The ratio of the impedance on the feedback loop to that on the signal input determined the gain, or amplification of the signal. The capacitor within the feedback loop on the pixel address and energy signals provided integration, helping to smooth the signal.

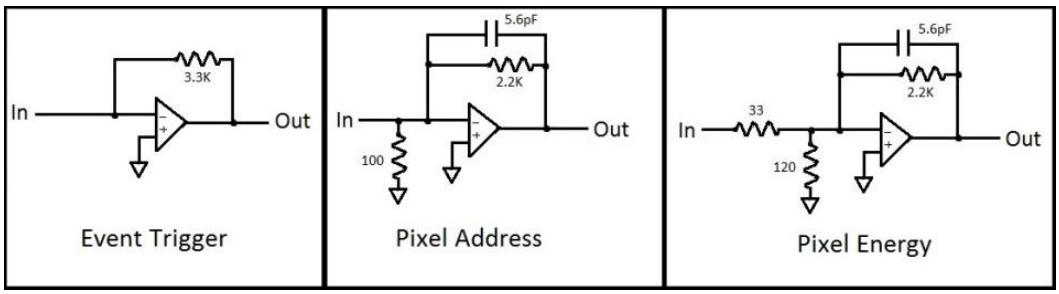

Figure 16. Schematic diagrams from LabRAT of each amplifier circuit. Values are listed for the resistors and capacitors. All inputs are connected to the inverting input of the amplifier.

The signal routing board did not have an equivalent in LabRAT like the detector carrier board did because its components replaced those from the DAB. Testing the board's operation required using a function generator and oscilloscope for input and output, respectively. A current signal for the input was approximated with a 0.05 V pulse at 20 kHz passed through a 10 pF capacitor. Electrical connections were difficult to establish for such small external signals, which complicated testing and debugging.

3.3 Heat Sink and Canister

The new detector head was housed in a tungsten canister (Figure 17) recycled from another project. The canister base measured 91 x 91 x 197 mm with a thickness of approximately 2.25 mm. The lid measured 91 x 91 x 25 mm. The aluminum lid of the canister was replicated in the machine shop because the original had a hole designed for a large diameter cable, while a ribbon cable was planned for the new system. A high voltage supply used for a previous project was adapted to suit the needs of the CZT modules and mounted to the inside of the lid. The bottom of the canister was lined with electrical tape to prevent the high voltage from coming in contact with the canister. The base was then covered with a square sheet of copper to provide high voltage to all CZT modules. A wire tacked onto the copper sheet with solder and clear glue was connected to the output of the high voltage supply (-600 V). The base of the canister also had an integrated collimator, a feature that was missing from LabRAT but is crucial for nuclear imaging applications.

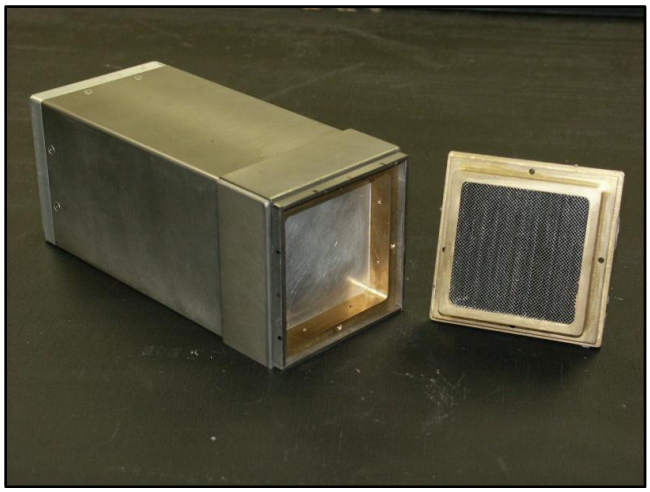

Figure 17. Canister, lid, and collimator. These components were originally used for an unrelated project. While the lateral dimensions were closely matched to the size of the new DCB, the canister length was actually longer than required. The circuit boards and heat sink frame occupy approximately half of the available volume inside the canister.

An aluminum frame (Figure 18) acted as a heat sink to draw heat away from the modules' ASICS. The frame included four corner supports that were screwed to the signal routing board, two cross beams to connect the corner supports, and two other cross beams to secure the heat sinks in place. Each piece was machined in-house to fit within the detector head. The heat sinks themselves were T-shaped so that the bottom of the heat sink had more surface area in contact with the back of the CZT module. Electrical tape was wrapped around the base of each to prevent the heat sinks from rubbing against the holes in the signal routing board and detector carrier board.

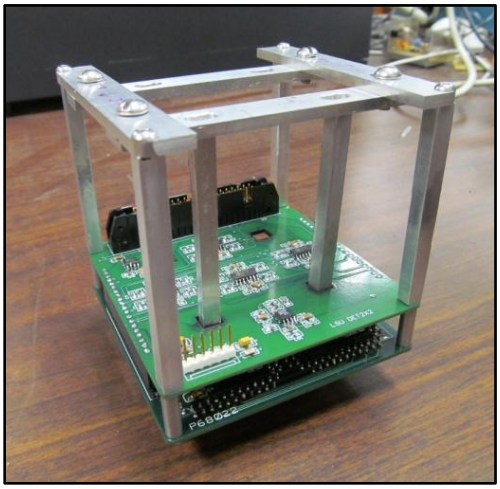

Figure 18. Assembled frame with two heat sinks in place. The signal routing board is visible on top of the detector carrier board. On the left side, one of the twenty-pin connectors is also visible between the boards.

The frame and boards fit snugly within the canister so that the aluminum frame was in contact with the tungsten. This configuration allowed for the tungsten canister to contribute to heat dissipation. The canister was approximately two times the length of the board and frame assembly. Thus, the interior volume could be reduced by half and still accommodate all of the components. However, tungsten is expensive and difficult to machine, so we chose not to modify

the canister or to construct a new one; instead the frame assembly was made larger than necessary to hold the CZT modules fixed within the canister.

4. Discussion and Conclusions

4.1 Summary of Project Tasks

This project encompassed many nontrivial tasks to adapt an existing gamma camera system for small field-of-view applications. Besides the construction of a new detector head, modifications to the system were necessary to facilitate interfacing. These tasks are grouped by component and listed below with their current status. All tasks were completed by the author except where noted.

- Detector carrier board
  - Board layout: complete (Ellison – Electronics Shop)
  - Fabrication: complete (outside vendor)
  - Population: complete
  - Testing: complete
- Signal routing board
  - Board layout: complete (Ellison – Electronics Shop)
  - Fabrication: complete (outside vendor)
  - Population: complete
  - Testing: complete
- Canister
  - High voltage plane: complete
  - Heat sinks: complete
  - Frame: complete
  - Back cover: complete (Machine Shop and author)
- DAB modification
  - Removal of components: complete (Electronics Shop)
  - Testing: in progress
- Software modification
  - Global module number: complete
  - Initialization file: complete

4.2 Challenges

Troubleshooting is a necessary aspect of any work with electronics. This chapter discusses problems that were discovered with elements of this project and solutions where they existed. Elements to be discussed include the detector carrier board, signal routing board, and

modified DAB. When the system was fully assembled but not functioning correctly, identifying the problem could be a difficult, time-consuming task. Using a multimeter, oscilloscope, and process of elimination usually narrowed down the culprit to a particular signal or circuit. Then, the component or process at fault was modified or replaced.

Very few problems were encountered with the detector carrier board. Two capacitors connected to the power were electrolytic capacitors and had to be oriented in the correct direction, which was not specified on the board itself. Care was taken to determine the correct orientation for each. Also, the board was found to be mislabeled for two components, discovered after a capacitor burned out. The board had the labels for "R21" and "C21" switched, so those two components were removed and replaced in the correct position. The heat sink cutouts were added to both the detector carrier board and the signal routing board by the Physics electronics shop. Additional copies of the boards were fabricated so that a backup was available.

Several problems were encountered with the signal routing board, including incorrect wiring and a missing ground connection. Schematics for the first version of the board misconnected a pin of the trigger circuit; the signal for the trigger was directed from the detector carrier board directly to the DAB, bypassing the op-amp entirely. We attempted to cut the unwanted trace on the board and add wires to the input and output of the amplifier, but the connections were not stable enough to carry the signal adequately. Thus, the schematics were redrawn correctly and a second version of the board was printed. After printing, close inspection of the DAB revealed a component that was not included in the schematics; the non-inverting input of the trigger op-amp was connected to ground through a 100 Ω resistor. This resistor was added to the signal routing board using test points located on the underside which faces the detector carrier board (Figure 15, left).

Staff of the Physics electronics shop removed the components of the DAB which were duplicated by the new signal routing board. Currently, the DAB which had components removed is undergoing investigation by the electronics shop. Problems in initialization were traced to the trigger circuit, which was not producing pulses of the correct size or shape at its output. Without a functioning trigger signal, initialization is completed incorrectly so that events do not register with the LabView software. Thus, LabView will run but each pixel appears to record no events, leading to blank image and energy displays.

Some errors commonly encountered during testing and operation included faulty soldering, incorrect power, and lack of daisy chains. Each op-amp had eight or fourteen pins that were individually soldered onto pads on the signal routing board. Soldering is an art that requires precision and delicacy, both of which are gained through experience; this was especially true when manually soldering modern small surface-mount components. Connections were tested using a multimeter, but sometimes the pressure of the probe provided enough force to make a poor connection better. Visual inspection of the board under a high power magnifying glass was the best tool in diagnosing soldering issues.

Power connections at the DAB and signal routing board were carefully monitored to ensure that op-amps are receiving the correct voltages. Power at the DAB was relatively easy to check because of a fuse and green LED connected to the positive and negative voltages. The LED would turn off when the fuse was blown by a higher voltage or the voltage is below its expected value. Power for the signal routing board was checked with a voltmeter. Incorrect voltages at the signal routing board connector could be due loose wires within the cable or problems with grounding. Power issues were the most common yet reparable problems that we encountered during testing of the system.

4.3 Conclusion

The construction of a compact gamma camera from an existing system provided insight into both the design and operation of gamma cameras. This project focused on the development of electrical and mechanical components of the detector head. A key aspect of this project was moving some signal processing electronics from the existing DAB board to a new board located in the detector head. While the design of the circuits on the new signal routing board was straightforward and followed typical design principles, we had no schematic layout of the existing DAB to use in planning modifications. This lack of documentation complicated both the implementation and debugging of changes to the DAB, becoming a significant portion of the effort on this project. However, the original DAB likely represented many person-months of design effort; reinventing all the DAB's features was deemed to greatly exceed the scope of an undergraduate honors thesis. Future work will entail investigation of the properties of the system, including image quality and energy resolution. The gamma camera will ultimately be used in small field-of-view applications where its compact size and mobility are necessitated.

References

[1]B.L. Franc et al. "Detection and localization of carcinoma within the prostate using high resolution transrectal gamma imaging (TRGI) of monoclonal antibody directed at prostate specific membrane antigen (PSMA) – Proof of concept and initial imaging results." Eur. J. Rad. **82**, 1877-1884 (2013).

[2]E.M. von Meyenfeldt et al. "Radionuclide-guided biopsy of bone lesions in cancer patients; A reliable, well-tolerated technique." Eur. J. Surg. Oncol. **40**, 193-196 (2014).

[3]M. Tsuchimochi et al. "A prototype small CdTe gamma camera for radioguided surgery and other imaging applications." Eur. J. Nucl. Med. Mol. Im. **30**, 1605-1614 (2003).

[4]S. Del Sordo et al. "Progress in the development of CdTe and CdZnTe semiconductor radiation detectors for astrophysical and medical applications." Sensors **9**, 3491-3526 (2009).

[5]A.E. Bolotnikov et al. "Material properties limiting the performance of CZT gamma-ray detectors." GOMAC Tech Conference (2009).

[6]C. Scheiber. "CdTe and CdZnTe detectors in nuclear medicine." Nucl. Inst. Meth. Phys. A **448**, 513-524 (2000).

[7]C. Mestais et al. "A new design for a high resolution, high efficiency CZT gamma camera detector." Nucl. Inst. Meth. Phys. A **458,** 62-67 (2005).

[8]D.J. Wagenaar. "CdTe and CdZNTe Semiconductor Detectors for Nuclear Medical Imaging." *Emission Tomography: the Fundamentals of PET and SPECT*. Edited by M.N. Wernick and J.N. Aarsvold (Elsevier Academic Press, 2004).

[9]A.E. Bolotnikov et al. "Performance-limiting defects in CdZnTe detectors." IEEE Nuclear Science Symposium (2006).

[10]J. Oddstig et al. "Reduced administered activity, reduced acquisition time, and preserved image quality for the new CZT camera." J. of Nucl. Card. **20**, 38-44 (2013).

[11]J.R. Tickner, M.P. Currie, G.J. Roach. "Feasibility study for a low-cost 3D gamma-ray camera." Applied Radiation and Isotopes **61**, 67-71 (2004).

[12]B. Herzog et al. "Nuclear myocardial perfusion imaging with a cadmium-zinc-telluride detector technique: Optimized protocol for scan time reduction." J. Nucl. Med. **51**, 46-51 (2010).

[13]L. Kelly."Performance evaluation of two CZT imaging systems." MS Thesis, Louisiana State University, 2005.

[14]P. Horowitz, W. Hill. "Horowitz and Hill: The Art of Electronics." (Cambridge University Press, 1980) 92-99.